Crystalline Forms and Emission Behavior of Poly(9,9-di-*n*-octyl-2,7-fluorene)

S. H. Chen, A. C. Su,* and C. H. Su

Institute of Materials Science and Engineering, National Sun Yat-sen University, Kaohsiung 804, Taiwan

S. A. Chen

Department of Chemical Engineering, National Tsing Hua University, Hsinchu 300, Taiwan

Received September 7, 2004; Revised Manuscript Received October 29, 2004

ABSTRACT: By means of transmission electron microscopy (TEM) and X-ray diffraction (XRD) we demonstrate the presence of a previously unspecified modification (α′) of the crystalline (α) phase in poly(9,9-di-*n*-octyl-2,7-fluorene) (PFO). The α′ form is metastable and lower in melting temperature than the α form, and its formation is kinetically favored at temperatures lower than 130 °C. The modification involves mainly a slight increase in the *b* axis from 2.34 to 2.38 nm and lowered symmetry along this axis, whereas the *a* axis tends to lie preferentially normal to film surface. Using specimens composed selectively of α and α′ phases, respectively, we show that films of the two forms are characteristically different in routine 1-D XRD profiles and absorption spectra. These are attributable to the oriented nature of the α′ form as well as minor but significant differences in molecular packing and backbone coplanarity. However, photoexcited emission spectra of these films remain highly similar in the vibronic structure to the purely nematic film, with only minute shifts in emission maxima that are inconsistent with the significantly red-shifted absorption edge upon crystallization. This appears better explained by assuming that the liquid-crystalline matrix rather than crystalline domains dominates optical emission of PFO.

Introduction

As one of the most extensively studied examples of semiconducting polymers,[1−3] poly(9,9-di-*n*-octyl-2,7-fluorene) (PFO, chemical structure given as inset in Figure 3b) is well known to be semicrystalline with a melting temperature near 160 °C, above which a nematic (N) phase exists up to ca. 300 °C.[4−7] A mesomorphic *β* phase may also exist upon solvent vapor treatment.[8,9] As these phases can be rather selectively maintained via proper selection of processing parameters,[4,8,9] the resulting morphology effects in light-emission properties of PFO have been extensively examined in the literature.[10−19] However, details of the molecular arrangement in these phases remained obscure,[9,18] rendering earlier attempts to establish a correlation between morphology and photophysical properties rather imprecise. Systematic clarification of the phase behavior of PFO is clearly needed. On the basis of transmission electron microscopy (TEM) and X-ray diffraction (XRD) observations, we recently[20] proposed a structural model for the α phase as orthorhombic (a = 2.56 nm, b = 2.34 nm, c = 3.32 nm, space group $P2_12_12_1$), with eight chains in the unit cell (each of four fluorene repeats) and theoretical density 1.041 g/dL.

As the α phase structure is better understood, here we show the previously unspecified presence of a closely related form (coined as the α′ phase), kinetically favored at crystallization temperatures (T_c) below ca. 130 °C. The modification mainly involves a slight increase in the *b* axis to 2.38 nm, lowered symmetry along this axis, as well as preferred orientation of the *a* axis along film normal. This oriented crystalline modification affects the typical 1-D XRD profile of PFO films in a characteristically distinct manner; it also results in a clearly red-shifted absorption edge. However, photoexcited emission spectra of the α′ film, the α film, and a reference film of purely N phase remain highly similar except for minute red shifts in the emission maximum. This is inconsistent with the clearly red-shifted absorption edge upon crystallization. It is therefore conjectured that crystalline domains, whatever their form, contribute insignificantly to photoexcited emission of PFO.

Experimental Section

The PFO sample used here was purchased from American Dye Source, Quebec, Canada (cat. no. ADS129BE). The weight-average molecular mass (M_w) was 65 kDa and polydispersity index PDI = 2.6 as determined via GPC using polystyrene standards. Since small-angle light-scattering results of Grell et al.[8] suggested a correction factor of $(2.7)^{-1} = 0.37$, the true M_w value is estimated to be 24 kDa.

Transmission electron microscopic (TEM) studies were performed using a JEOL 3010 instrument under an acceleration voltage of 200 kV at which the combined factor of wavelength and camera length has been carefully calibrated using (111), (200), (220), and (311) reflections from vapor-deposited Al thin film. For the X-ray diffraction (XRD) studies, a Bruker D8 Advance diffractometer equipped with a copper target (Kα line, with wavelength λ = 0.154 nm), a graphite collimator, and a vacuumed high-temperature stage (Anton Paar TTK-450) was used under a step−scan rate of 0.05° per 3 s in the scattering angle range of 2θ = 1−41°. Full-range calibration of the scattering angle was made using both silicon and silver behenate standards. Optical absorption (UV−vis) and photoluminescence (PL) spectra of the film specimens were obtained using a Hong-Ming MFS-230 instrument, which is traditional in design except that excitation and signal collection are through optical fibers such that, with slight changes in the positioning of optical fibers and the orientation of the sample holder, both absorption and emission measurements can be made. Differential scanning calorimetric (DSC) mea-

* To whom correspondence should be addressed. E-mail: acsu@mail.nsysu.edu.tw.

10.1021/ma048162t CCC: $30.25
Published on Web 12/21/2004

surements were made using a TA Q100 instrument routinely calibrated using indium and lead standards and operated under a stream of nitrogen gas.

Films were drop cast from dilute solutions of PFO in toluene on glass or quartz substrates. The adopted concentration was ca. 0.1 w/v % or lower for TEM and UV−vis/PL specimens with the substrate tilted nearly vertically right after solution dropping to give films of ca. 0.1 mm in thickness; films for XRD studies were much thicker (ca. 50 μm) using a higher concentration of 0.2 w/v % and repeated drop casting at the same area on the substrate. The as-cast films were then routinely vacuum dried (in excess of 4 h at ca. 80 °C) before further heat treatments at elevated temperatures. These were *routinely* started by a brief 1-min treatment at 250 °C to eliminate previous processing history. This was followed by jumping to 140 °C for long-term (40 min or longer) crystallization and subsequent quenching into ice water to obtain films selectively rich in the α form. For films selectively rich in the α′ form, a temperature jump from 250 to 160 °C and subsequently programmed cooling at 20 °C/min to room temperature were adopted. All heat treatments were made in an ice-water-cooled high-temperature stage (Linkman THMS-600, connected to a TMS-91 temperature controller) under protective nitrogen atmosphere. It should be emphasized here that these specimens were in essence only semicrystalline;[21] the use of terms such as "films of the α form" or "the α film" are only convenient abbreviations for "films composed of the α phase within a nematic matrix". For comparison purposes, nematic films were prepared by direct quenching from 250 °C into ice water,[22] and films of mesomorphic β phase were prepared by allowing slow evaporation of toluene under a toluene-rich atmosphere.

TEM specimens were detached from the glass substrate using a dilute HF solution. In the case of shear-oriented specimens, a manual shearing procedure (i.e., sweeping a blade over the melted thin film) was adopted prior to the heat treatment steps. These specimens were then vapor-deposited with carbon or shadowed (with an incidence angle of 60° from plane normal) with a combined Pt/C source prior to TEM examinations.

Results

Selective Formation of the α and α′ Forms. Given in Figure 1a is a representative bright-field image (BFI) and the corresponding selected area electron diffraction (SAED) pattern of shear-oriented specimens of isothermally crystallized (1 h at 140 °C, followed by quenching to 0 °C) α phase. The SAED pattern dictates backbone orientation along the shear direction, which is transverse to thin stripes approximately 25 nm in spacing. We note that this pattern is in full agreement with the fiber XRD pattern previously given by Grell et al.[9] All diffraction spots may then be consistently indexed (cf. Figure 1c) according to the orthorhombic unit cell structure reported previously.[20] Note that the (*0k0*) spots in this unit cell structure are relatively weak, with intensities decreasing in the order of $I_{060} > I_{040} > I_{020}$ (cf. the corresponding [*00l*] zone pattern, Figure 1c in ref 20); hence, the latter two reflections are indiscernible along the equator in this "fiber" pattern.

In the case of programmed cooling at 20 °C/min from the nematic state, however, peculiar observations emerge. The BFI and the SAED pattern in Figure 1b indicate features of both the backbone alignment in the direction of shear and the transversely oriented thin stripes, which are more or less similar to those shown in Figure 1a. However, equatorial spots other than the (*0k0*) series with even *k* are all missing, whereas relative intensities of off-axis (*0kl*) spots with even *k* are clearly enhanced (cf. Figure 1d). Simple tilting of the specimen by ca. 38° (cf. Figure 1e) brought out the missing equatorial spots, suggesting 3-D orthorhombic order. The 38° tilt is consistent with progression from the [*001*] zone to the [*101*] zone. This means that with the *c* axis parallel to shear direction, the *a* axis of the shear-aligned crystalline phase is now further oriented along the film normal. However, a closer comparison between the fully indexed SAED patterns in Figure 1c and d indicates that the *b* axis is slightly increased from 2.34 to 2.38 nm. More importantly, the intensity enhancement in (*0k0*) reflections implies lowered symmetry along the *b* axis, which represents a minor yet crystallographically significant difference. Nevertheless, as the two structures are indeed largely similar, this new structure with a preferred orientation of the *a* axis along film normal is considered a modified form of the α phase and coined the α′ form. It should be noted that the aperture size adopted was ca. 0.3 μm, much larger than the coherence lengths (50 nm or lower) given by Grell et al.[9]

Kinetic Preference vs Thermodynamic Stability. Given in Figure 2a are characteristic XRD profiles for films selectively composed of N, β, α, and α′ phases. The N film (quenched from 250 to 0 °C) is featureless except for weak and broad halos centered at $2\theta = 5.5°$ and 20° (corresponding to *d*-spacing values of 1.6 and 0.44 nm, respectively). In the as-cast state, the β-rich film is characterized by a single broad peak centered around $2\theta = 7.3°$ (i.e., 1.21 nm in *d* spacing). More detailed structural analysis and morphological observations of these noncrystalline phases are postponed to a later date.[23] The XRD profile of the α film is characterized by sharp and clear peaks in full accord with the orthorhombic unit cell structure, as discussed previously.[20] In contrast, the XRD profile of the α′ film is characterized by the prominence of (200) reflection and the absence of (110) and (210) reflections in the lower angle range. This is consistent with the assigned orientation that the *a* axis of the α′ phase lies normal to the film surface: only the (*h*00) planes with even *h* strictly satisfy the Bragg condition in the reflection-type diffractometer geometry. Presented in Figure 2b is the powder-like SAED pattern (which correspond to transmission geometry) with the aperture removed from the electron beam (ca. 10 μm in diameter) path. The dominance of (*0kl*) rings with even *k* is clearly observed, in support of our interpretation that the *a* axis is preferentially oriented along the film normal.

Presented in Figure 3a and b are two sets of XRD profiles of an α′ film that was subjected to a series of stepwise heating (Figure 3a) and the subsequent stepwise cooling experiments in intervals of 15 °C. It may be observed from Figure 3a that reorganization of the α′ form into the α form may be observed at temperatures above 115 °C. This is followed by complete melting of the α form at 160 °C, for which the XRD profile is not shown but is similar to the 145 °C profile in the cooling sequence (cf. Figure 3b). The subsequent stepwise cooling from the nematic phase results in more a fully developed α phase. Figure 3c more clearly shows minor yet significant increases in the relative intensity of the (200) reflection during stepwise cooling from 145 °C in 15 °C intervals, indicating kinetically favored formation of the α′ modification below 130 °C. Upon further stepwise reheating the α′ phase melts in a lower temperature range, as indicated by the decrease in I_{200} from 132 to 152 °C in Figure 3d. This corresponds to the low-temperature shoulder near 140 °C in DSC heating traces (Figure 4a) upon repeated cycling be-

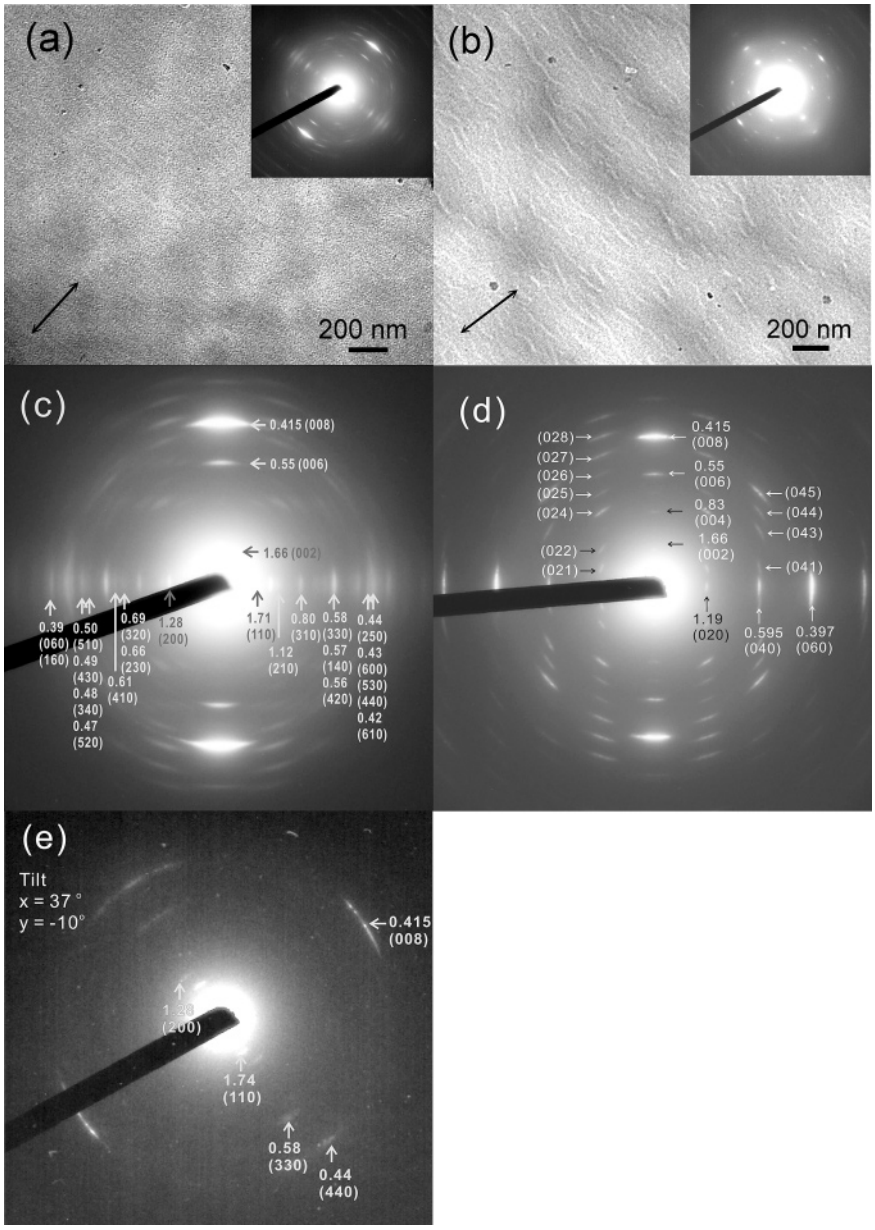

Figure 1. BFIs and the corresponding SAED "fiber" patterns of shear-oriented films: (a) the α phase (sheared at 250 °C; followed by 1 h crystallization at 140 °C, and then quenched to 0 °C), (b) the α′ modification (sheared at 280 °C, cooled from 160 °C at 20 °C/min, carbon coated), (c) indexed "fiber" pattern of the α phase, (d) indexed "fiber" pattern of the α′ modification, and (e) specimen tilted by 38° to show the equatorial "missing spots" in d. The adopted aperture size here was 0.3 μm in diameter.

tween 30 and 310 °C at 20 °C/min. Note that the prominent endotherm at 156 °C corresponds to the melting of the α phase, as indicated by XRD results in Figure 3. Partial reorganization of the melted α′ phase into the α form must have occurred, as the specimen at this cooling rate of 20 °C/min was dominantly composed of α′ crystals (cf. Figure 2a), which is also supported by a single sharp crystallization exotherm around 90 °C in the cooling cycle (Figure 4b). For curious readers, we note further that the endotherm around 80 °C and the following exotherm around 120 °C in the first heating trace of the as-received sample is related to dissipation of the solvent-induced mesomorphic β phase and subsequent transformation into crystalline order. This is to be elaborated in a future article.[23]

Optical Absorption. Given in Figure 5a are area-normalized absorption spectra of films composed mainly of N, β, α, and α′ phases. With the absorption maximum located near 385 nm, a rather symmetric broad band spanning from 320 to 430 nm characterizes the optical absorption of the N phase. The main absorption of the α film is similar to that the N film except for some broadening toward long wavelengths, resulting in a red-shifted absorption edge at 440 nm. In comparison, the β film exhibits a narrower main absorption and a clearly developed peak around 430 nm, extending the absorption edge to 445 nm. This particular peak at ca. 430 nm has been considered characteristic of the β phase in the literature. However, although the width of the main absorption remains similar to N and α phases, a similar peak exists at a slightly shorter wavelength for the α′ films, extending the absorption edge to 445 nm. Similar observations have been reported previously[9,24,25] but with more attention paid to the solvent-induced β phase rather than the possible existence of a metastable crystalline form.

The redistribution in conjugation length is more clearly identifiable in the difference spectra (using the

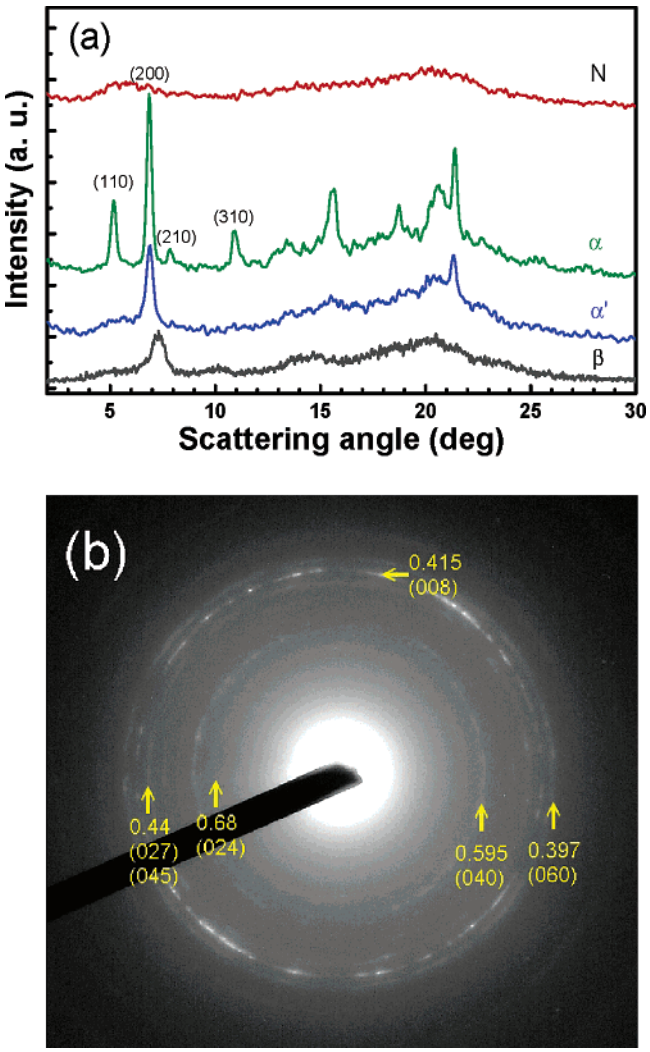

Figure 2. (a) Characteristic XRD profile (obtained under reflection geometry) for films rich in N, α, α′, and β phases, respectively. (b) SAED powder-like pattern (which corresponds to transmission geometry) for the α′ film without using the aperture (beam diameter = ca. 10 μm). The dominance of (*0kl*) rings with even *k* is clearly observed, indicating that the *a* axis is indeed preferentially oriented along the film normal.

absorption spectrum of the N film as a common base) given in Figure 5b. The α∠N curve shows increased absorptions centered at 423 nm with decreased absorptions in the range of 350−410 nm; the maximum loss of optical density, however, occurs at the long-wavelength range around 405 nm. In the case of the α′−N curve, strong increases in optical density are observed centered around a slightly longer wavelength of 426 nm. Decreased optical absorptions are also observed in the range of 350−410 nm, but the maximum loss in optical density shifts to a shorter wavelength of ca. 375 nm. These observations indicate that formation of the α phase results in improved conjugation for chain segments that are already of comparatively extended conjugation; in contrast, formation of the α′ phase brings segments of comparatively poor conjugation into better coplanarity. As compared to the α phase, further (although slight) extension in conjugation length in the α′ phase may probably be related to the increased *b* axis that results in less restrictions in the development of backbone coplanarity. In comparison, the β film exhibits higher populations around 433 nm and in the range of 370−400 nm with decreased optical density mainly in the short-wavelength range (<370 nm) as well as in a narrow range of 410−420 nm. This means that transformation from N to β phase involves a general increase in conjugation length, but the regions of longer conjugation length are further extended to give the additional peak around 430 nm.

Photoexcited Emission. In contrast to dramatic differences in the XRD profiles, the emission spectra of the N, α, and α′ films are highly similar (cf. Figure 5c) except for slight red shifts (successively by 2−3 nm) in emission maxima near 430, 455, and 490 nm. It is then interesting to note that the strongest emission around 430 nm is shorter in wavelength than the corresponding absorption edges of 440 and 445 nm for the α and α′ films, respectively. (For the sake of consistency, the absorption edge here is operationally defined as the intersection of extrapolated lines from both the inflection point of the high-wavelength branch of the main absorption peak and the absorption baseline above 450 nm. This procedure provides only a lower-bound estimate to the wavelength of the absorption edge but nevertheless eliminates difficulties in determining the precise point of first deviation from baseline. We re-emphasize that the prominent emission maximum is significantly shorter in wavelength than the corresponding absorption edge that is supposedly of underestimated wavelength.) This means that segments of highly extended conjugated conformation in the crystalline state contribute insignificantly to optical emission due to longer lifetime and poorer efficiency. Neither the second nor the third emission peaks attributable to segments of extended conjugation near the absorption edge as the consecutive red shifts of 5 nm in absorption edges between N and α phases or α and α′ phases are sufficiently reflected. If we consider these are as phonon sidebands of the main peak near 430 nm, the coupling mode would lie in a rather wide range (1300−1500 cm^{-1}) in vibration frequency. We note further that the relative intensities at ca. 455 and 490 nm cannot be explained by a straightforward Franck−Condon analysis using a single Huang−Rhys parameter[26] as in the case of poly(2-methoxy-5-(2′-ethylhexyloxy)-1,4-phenylenevinylene) (MEH−PPV).[27] It is more likely that several phonon modes[12,18,28] are coupled to the electronic transition.

Photoexcited spectrum of the β film is comparatively simple: red-shifted emissions at 438, 466, and 497 nm may be attributed to vibronic features with a coupled phonon frequency of 1355 ± 15 cm^{-1}. Nevertheless, the relative intensities of the peaks still deviate from those predicted using a single Huang−Rhys parameter; this is attributed to stronger reabsorption effect for the emission at 438 nm. More importantly, the red shift in the 0−0 emission peak, i.e., from 429 nm for the α′ film to 438 nm for the β film, is inconsistent with the shared absorption edge of 445 nm. In addition, emission spectra of N, α, and α′ films in relative peak positions and intensities (cf. inset of Figure 4c) are surprisingly similar. These observations lead to the speculation that all emissions in these three specimens are from uncrystallized segments in the nematic phase, differences in emission maxima simply reflect different backbone conformations "frozen-in" at different temperatures (250 °C for the N film, 140 °C for the α film, and presumably near the T_g value of PFO at ca. 70 °C for the α′ film). As is well known, increased rotational freedom of backbone rings at higher temperatures generally results

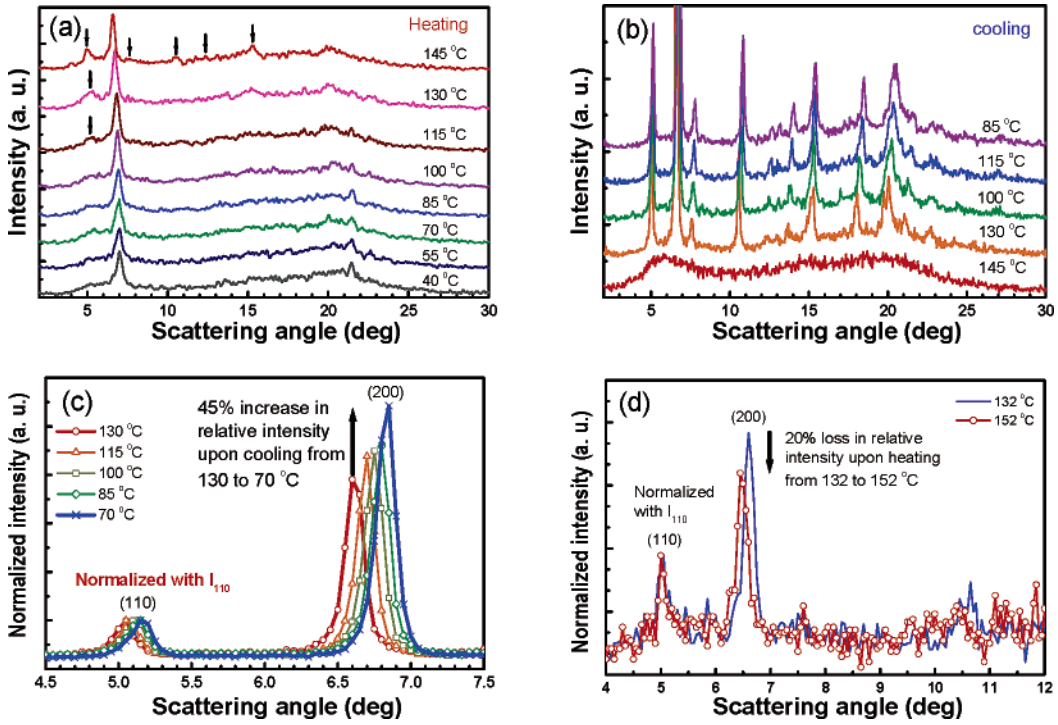

Figure 3. High-temperature XRD profiles upon stepwise changes in temperature obtained during (a) heating (room temperature to 160 °C, in intervals of 15 °C) and (b) cooling (160 °C to room temperature, in intervals of 15 °C) sequences. (c) Normalized XRD profiles to demonstrate the increase in the relative intensity of the (200) reflection due to kinetically favored formation of the α′ form below 130 °C upon stepwise cooling from 145 °C in intervals of 15 °C. (d) Normalized XRD profiles showing that the α′ phase melts at relatively low temperatures, as indicated by the decreased relative intensity of (200) reflection upon further stepwise increase in temperature from 132 (open circles) to 142 °C (filled squares). Data collection for each profile took ca. 40 min. The specimens were prepared via repeated drop casting and ca. 50 μm in thickness; the substrate was (amorphous) cover glass.

in decreased coplanarity and thermochromic effects. In other words, crystalline domains contribute little to photoexcited emission. In a recent report on aging of MEH−PPV solutions upon storage, formation of microcrystalline cross-links was shown to be responsible for gelation yet without discernible contributions to the emission spectrum.[29]

Discussion

Comparison with Friction-Transferred Film. With the structure and properties of the α′ form identified, it is then interesting to note that there is a recent report by Misaki et al.[30] on the "single-crystal-like" SAED pattern obtained from friction-transferred "crystalline" PFO films slowly cooled (0.2 °C/min) from 200 °C, although no detailed unit cell parameters or molecular packing were provided. We believe that this "single-crystal-like" SAED pattern corresponds to the α′ form discussed here as it essentially coincides with the SAED "fiber pattern" presented in Figure 1d. It might first appear surprising for general readers that shear action during the friction-transfer process and subsequent heat treatment could result in single-crystal-like features. However, in terms of our present picture, use of the term "single-crystal-like" is quite justifiable in view of the preferential orientation of the *c* axis along the shear direction and the kinetically favor alignment of the *a* axis along the film normal; these leave the *b* axis also specifically oriented perpendicular to the ***ac*** plane in terms of the orthorhombic unit cell structure.

There are minor differences in the two SAED patterns though. First, the *d*-spacing values are slightly different: in terms of the orthorhombic unit cell structure we proposed, their *d*-spacing values of 0.42 and 1.17 nm

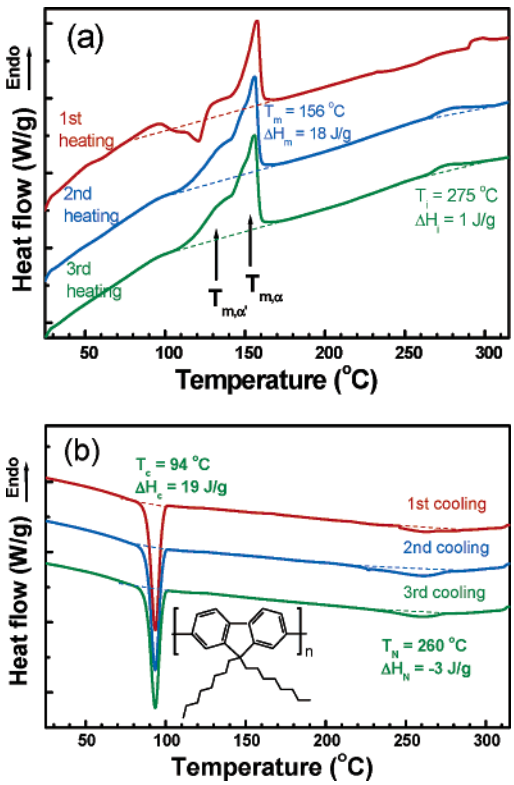

Figure 4. (a) DSC heating traces upon repeated cycling between 30 and 310 °C at 20 °C/min showing the low-temperature shoulder near 140 °C. (b) Corresponding DSC cooling traces showing crystallization at rather low temperatures near 90 °C under the programmed cooling rate of 20 °C/min. Some extent of reorganization of the partially melted α′ form into the high-melting α form must have occurred in a.

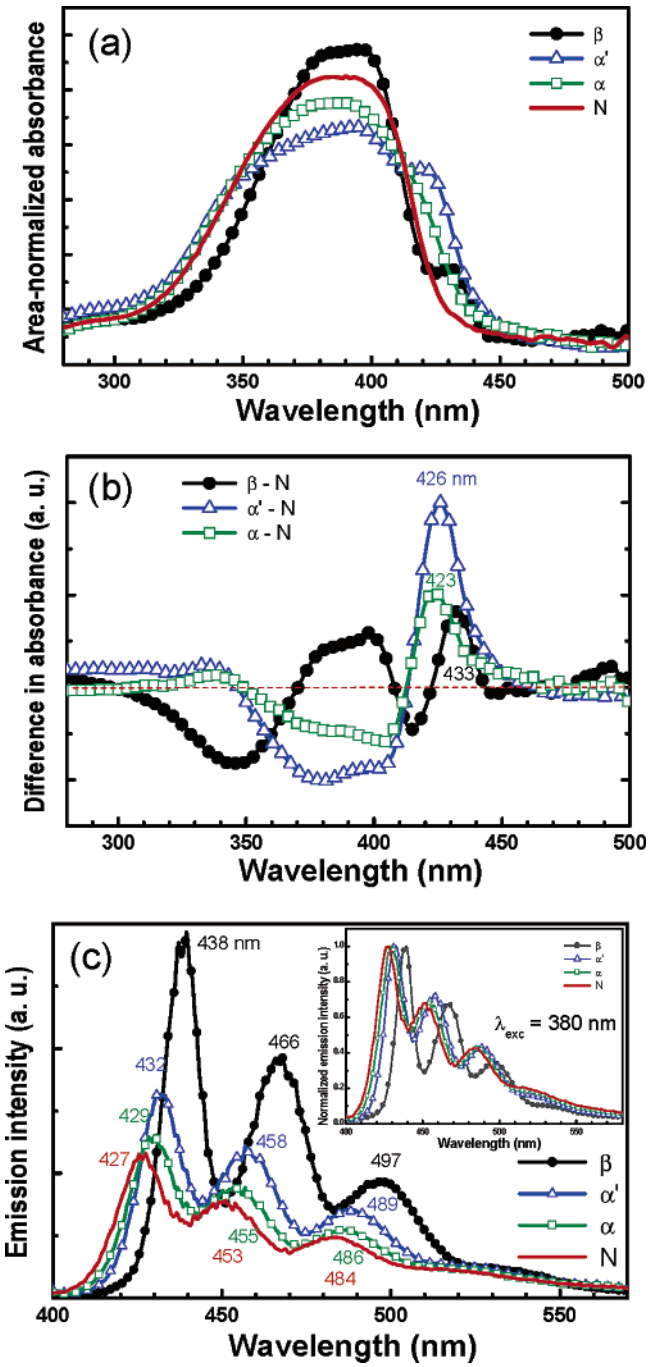

Figure 5. (a) Area-normalized absorption spectra of N, β, α, and α′ film specimens, (b) corresponding difference spectra using the spectrum of the N film as a common base, and (c) emission spectra of N, β, α, and α′ films with the normalized counterparts given as inset to show similarities among spectra of N, α, and α′ films except for slight and nearly parallel red shifts. The same piece of thin film (ca. 0.1 μm in thickness to minimize reabsorption effects) was used for all the UV−vis and PL measurements for the sake of self-consistency.

for the (008) and the (020) reflections are, respectively, greater and smaller than our corresponding values of 0.415 and 1.18 nm in Figure 1d. These differences may be attributed to the much greater shear stresses involved in their friction-transfer process and hence are crystallographically minor, as characteristic features of strong (*0k0*) with even *k* along the equator and strong (*0kl*) spots with even *k* remain similar in the two patterns. In addition, stray spots in their SAED patterns may arise (cf. their Figure 3f and Figure 4 in ref 30) that are attributed to distortion but, in our opinion, are more likely related to the minor presence of α grains (with the *c* axis oriented in the shear direction) in view of the comparative large (micrometer-sized) areas[30] selected for electron diffraction. This is also consistent with the slow cooling rate of 0.2 °C/min adopted for specimen preparation: this would result in ca. 18 min of residence time at temperatures between 145 and 130 °C, during which formation of some α crystals are rather likely as shown previously[20] and demonstrated here in Figure 2.

The "crystalline" film in the work of Misaki et al.[30] exhibited a shoulder near 415 nm with the absorption edge red shifted from 430 nm for the "liquid-crystalline" (rapid cooled from 200 °C, cooling rate unspecified) film to 435 nm, whereas the emission maximum is blue shifted from 434 nm for the "liquid-crystalline" film to 432 nm (cf. Figure 2 therein). All the spectroscopic features of their "crystalline" films are in better agreement with our results for α′ film rather than the α film. More importantly, the apparently inconsistent shifts in the absorption edge and emission maximum upon crystallization may be simply explained by the conjecture that crystalline domains contribute little to photoexcited emission. In our picture, the red shifted absorption edge is due to formation of crystalline domain, whereas the blue shift in the emission maximum may be accounted for by the difference in "frozen-in" temperature (somewhat lower than 200 °C vs ca. 70 °C) of the backbone conformation of the nematic matrix.

Similarity in Absorption Spectra and 1-D XRD Profiles of α′ and *β* Phases. As described in the previous section, the α′ phase is characterized by (1) strong (*0k0*) and (*0kl*) reflections with even *k* as well as disappearance of the (*200*) reflection in the normal-incidence diffraction pattern, (2) disappearance of (110) and (210) reflections (i.e., leaving only the (200) reflection with $d_{200} = 1.28$ nm in the lower angle region) in typical 1-D XRD profiles, and (3) presence of a relatively sharp optical absorption around 426 nm. Some of these characteristics are similar to those suggested in the literature for the solvent-induced β phase: these include the presence of a sharp optical absorption at ca. 430 nm and the appearance of a prominent reflection with an estimated[7,18] *d* spacing of 1.28 nm in XRD profiles obtained under grazing incidence[7] or routine measurements using reflective geometry of typical powder diffractometers.[18] As demonstrated for the two crystalline forms here as well as the comparison with results[27] of friction-transferred PFO films, an absorption peak around 430 nm is only indirectly related to the phase structure. As for the XRD profile, our recent results[23] indicated a lamellar structure with a layer spacing of ca. 1.22 nm, but there could be some variations in layer spacing under different processing conditions due to its mesomorphic nature. It is therefore rather unfortunate that these two "indirect criteria" (instead of more rigorous structural evidence such as a 2-D diffraction pattern) have been frequently used for typical identification of the β phase in the literature. We would therefore like to call for caution that some of the previous assignments for the β phase might possibly be the α′ phase reported here.

Acknowledgment. Financial support from the Ministry of Education and the National Science Council under contracts 91E-FA04-2-4A and NSC92-2216-E-110-009, respectively, are gratefully acknowledged.

References and Notes

(1) Kraft, A.; Grimsdale, A. C.; Holmes, A. B. *Angew. Chem., Int. Ed. Engl.* **1998**, *37*, 402.
(2) Neher, D. *Macromol. Rapid Commun.* **2001**, *22*, 1365.
(3) Scherf, U.; List, E. J. W. *Adv. Mater.* **2002**, *14*, 477.
(4) Grell, M.; Bradley, D. D. C.; Inbasekaran, M.; Woo, E. P. *Adv. Mater.* **1997**, *9*, 798.
(5) Teetsov, J.; Fox, M. A. *J. Mater. Chem.* **1999**, *9*, 2117.
(6) Blondin, P.; Bouchard, J.; Beaupre, S.; Belletete, M.; Durocher, G.; Leclerc, M. *Macromolecules* **2000**, *33*, 5874.
(7) Kawana, S.; Durrell, M.; Lu, J.; Macdonald, J. E.; Grell, M.; Bradley, D. D. C.; Jukes, P. C.; Jones, R. A. L.; Bennett, S. L. *Polymer* **2002**, *43*, 1907.
(8) Grell, M.; Bradley, D. D. C.; Long, X.; Chamberlain, T.; Inbasekaran, M.; Woo, E. P.; Soliman, M. *Acta Polym.* **1998**, *49*, 439.
(9) Grell, M.; Bradley, D. D. C.; Ungar, G.; Hill, J.; Whitehead, K. S. *Macromolecules* **1999**, *32*, 5810.
(10) Redecker, M.; Bradley, D. D. C.; Inbasekaran, M.; Woo, E. P. *Appl. Phys. Lett.* **1999**, *74*, 1400.
(11) Lee, J. I.; Klaerner, G.; Miller, R. D. *Synth. Met.* **1999**, *101*, 126.
(12) Ariu, M.; Lidzey, D. G.; Bradley, D. D. C. *Synth. Met.* **2000**, *111*−*112*, 607.
(13) Herz, L. M.; Phillips, R. T. *Phys. Rev. B* **2000**, *61*, 13691.
(14) Cadby, A. J.; Lane, P. A.; Mellor, H.; Martin, S. J.; Grell, M.; Giebeler, C.; Bradley, D. D. C.; Wohlgenannt, M.; An, C.; Vardeny, Z. V. *Phys. Rev. B* **2000**, *62*, 15604.
(15) Ariu, M.; Lidzey, D. G.; Lavrentiev, M.; Bradley, D. D. C.; Jandke, M.; Strohriegl, P. *Synth. Met.* **2001**, *116*, 217.
(16) Ariu, M.; Lidzey, D. G.; Sims, M.; Cadby, A. J.; Lane, P. A.; Bradley, D. D. C. *J. Phys.: Condens. Matter* **2002**, *14*, 9975.
(17) Korovyanko, O. J.; Vardeney, Z. V. *Chem. Phys. Lett.* **2002**, *356*, 361.
(18) Winokur, M. J.; Slinker, J.; Huber, D. L. *Phys. Rev. B* **2003**, *67*, 184106.
(19) Khan, A. L. T.; Banach, M. J.; Köhler. A. *Synth. Met.* **2003**, *139*, 905.
(20) Chen, S. H.; Chou, H. L.; Su, A. C.; Chen, S. A. *Macromolecules* **2004**, *37*, 6833.
(21) Our preliminary results from small-angle X-ray scattering results indicated a maximum level of crystallinity around 40%.
(22) Here we assume that heat treatment at 250 °C is sufficient for erasing all previous thermal histories. Our preliminary results from combined DSC and SAXS studies indicated that the equilibrium melting temperature of PFO is ca. 185 °C.
(23) Chen, S. H.; Su, A. C.; Chen, S. A. Submitted to *J. Phys. Chem. B*.
(24) Ariu, M.; Sims, M.; Rahn, M. D.; Hill, J.; Fox, A. M.; Lidzey, D. G.; Oda, M.; Cabanillas-Gonzalez, J.; Bradley, D. D. C. *Phys. Rev. B* **2003**, *67*, 195333.
(25) Cheun, H.; Tanto, B.; Chunwaschirasiri, W.; Larson, B.; Winokur, M. J. *Appl. Phys. Lett.* **2004**, *84*, 22.
(26) Pope, M.; Swenberg, C. E. *Electronic Processes in Organic Crystals and Polymers*, 2nd ed.; Oxford University Press: Oxford, 1999.
(27) Chen, S. H.; Su, A. C.; Chou, H. L.; Peng, K. Y.; Chen, S. A. *Macromolecules* **2004**, *37*, 167.
(28) Khan, A. L. T.; Sreearunothai, P.; Herz, L. M.; Banach, M. J.; Koehler, A. *Phys. Rev. B* **2004**, *69*, 085201.
(29) Chen, S. H.; Su, A. C.; Chang, C. S.; Chen, H. L.; Ho, D. L.; Tsao, C. S.; Peng, K. Y.; Chen, S. A. *Langmuir* **2004**, *20*, 8909.
(30) Misaki, M.; Ueda, Y.; Nagamatsu, S.; Yoshida, Y.; Tanigaki, N.; Yase, K. *Macromolecules* **2004**, *37*, 6926.

MA048162T